applied sciences

MDPI

Article

Prediction of Machining Deformation for Split Equal-Base Circle Bevel Gear

Kai Xu [1,2,3], Ying Xiao [1,*], Wen Xin [4], Bo Cheng [4] and Bin Wang [1,2,3]

[1] School of Mechatronics Engineering, Henan University of Science and Technology, Luoyang 471003, China; x62025@126.com (K.X.); 9902848@haust.edu.cn (B.W.)
[2] Longmen Laboratory, Luoyang 471000, China
[3] Collaborative Innovation Center of Henan Province for High-End Bearing, Henan University of Science and Technology, Luoyang 471000, China
[4] CITIC Heavy Industries Co., Ltd., Luoyang 471039, China; xinwen@citic-hic.com.cn (W.X.); chengbo@citic-hic.com.cn (B.C.)
* Correspondence: xiaoy190791@gmail.com

Abstract: Given the deformation issues in machining segmented equal-base bevel gears, this paper investigates the variations of additional stress during the machining process, considering the gear blank material, residual internal stress, and gear blank design. A model for calculating internal additional stress and torque during gear machining has been developed. The calculation formula for the bending deformation of the gear blank has been derived using the torque–area method. By analyzing the time-varying stiffness of the blank, a calculation model for the bending deformation of the gear blank has been constructed, and the projection analysis of gear stock deformation has been completed. Based on the cumulative superposition effect of its deformation projection, a calculation model for the overall deformation of the segmented gear blank has been formulated. The deformation calculation model has been validated through finite element simulation, deformation calculation, actual machining, and measurement verification.

Keywords: segmented equal-base bevel gears; machining deformation; internal stress; finite element simulations

check for updates

Citation: Xu, K.; Xiao, Y.; Xin, W.; Cheng, B.; Wang, B. Prediction of Machining Deformation for Split Equal-Base Circle Bevel Gear. *Appl. Sci.* **2024**, *14*, 5645. https://doi.org/10.3390/app14135645

Academic Editor: Arkadiusz Gola

Received: 7 May 2024
Revised: 22 June 2024
Accepted: 25 June 2024
Published: 28 June 2024

Copyright: © 2024 by the authors. Licensee MDPI, Basel, Switzerland. This article is an open access article distributed under the terms and conditions of the Creative Commons Attribution (CC BY) license (https://creativecommons.org/licenses/by/4.0/).

1. Introduction

Extra-large bevel gears play a crucial role in heavy industrial equipment across mining, power generation, and other sectors. Particularly, when the diameter exceeds 3000 mm, the processing methods and machining equipment become highly demanding, leading to increased complexity in testing equipment and methods. Consequently, manufacturing becomes challenging, expensive, and time-consuming. To address these challenges and facilitate transportation and machining, split straight bevel gears are widely employed in existing heavy industrial equipment. The equal-base circle bevel gear is a unique type of curved-tooth bevel gear in China [1–3]. Its machining principle is straightforward, making it particularly suitable for small machine tools to process large gears. Moreover, it is easily divisible. Hence, the large-size equal-base -bevel gear proves to be a superior alternative to the super-large straight bevel gear.

Upon processing the split gear blank, engineering practices and existing data indicate that its deformation typically reaches the millimeter level [4,5]. The main reason for this is the shape change in the response accuracy of large bevel gears. The change in stiffness and the removal of materials then play a major role in the gear blank structural deformation, causing 92.2% of total deformation. The structural deformation of the wheel blank is closely related to its section design and how to divide the overall wheel. However, the gear blank is divided first and then cut, so the deformation is large. In the existing manufacturing process, there is no design standard, and human factors have a great influence on the rational design and segmentation of gear blanks.

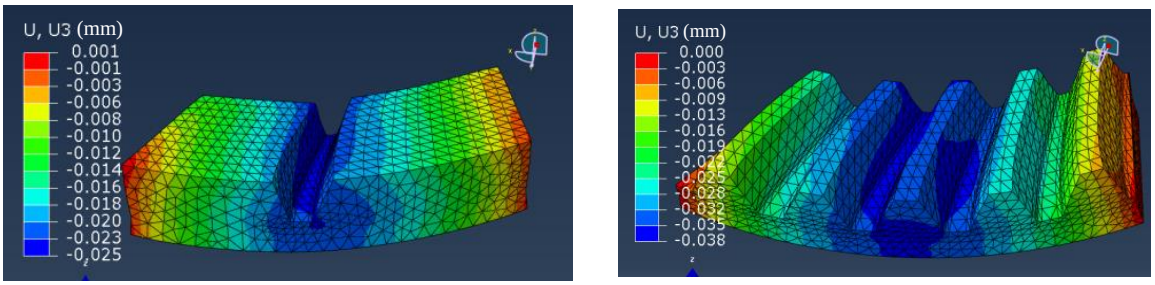
Therefore, based on the gear blank material and the geometric gear parameters, a deformation prediction model is established, and the model is suitable for predicting the structural deformation of gear blanks, which will be very important for split equal base bevel gear. However, the existing research assumes that the gear blank is integral, with no exploration of internal stress changes, stiffness variations, and deformation calculations. In the research domain of split large gears, the primary focus is on large cylindrical gears, particularly emphasizing processing technology, deformation control methods, and deformation mechanisms [6]. Wang et al. [7] studied the laws of internal stress changes during the machining of split-type straight bevel gears and discussed the internal deformation mechanism and laws of split-type straight bevel gears. Sun et al. [8] of Zhejiang University, through theoretic calculation and ABAQUS modeling simulation, solved the deformation of a rectangular section beam under unidirectional stress in the process of delamination and studied the deformation of a large integral structure caused by residual stress of the blank after NC machining. The results show that the theoretical solution is consistent with the finite element calculation. Meng et al. [9] studied the residual stress of machined parts by using the "life and death element" technology of finite element software and simulating stress peeling. Wang et al. [10] studied the stress superposition and redistribution by establishing the finite element model of the deformed workpiece and analyzed the principle of the machining deformation of structural parts. Huang et al. [11] analyzed the relationship between stress redistribution, stiffness change, and the deformation of aeronautical integral structural parts during machining and established the model to predict the deformation of integral components. Nervi [12] established a model for predicting machining deformation of parts with internal stress and analyzed how the initial internal stress distribution affects the deformation. Keith [13] studied the effect of machining stress on part deformation during machining. Ratchev et al. [14] established a neural network model for thin-walled parts to predict their machining errors. Takayuki AOYAMA et al. [15] analyzed the plastic deformation mechanism of hypoid gears caused by internal stress under the line of contact through finite element analysis. ABDUL AZIZ et al. [16] studied stress and deformation in reinforced structures obtained using a layered machining method.

Thus, our research was conducted according to these aspects. First, the deformation and additional stress analysis of equal-base circle bevel gear blank in the process of gear cutting were performed, and the calculation model of additional torque in the residual material of the blank was established. Then, the formula to calculate deformation was deduced, and the projection analysis of wheel blank deformation was performed. Finally, based on the superposition effect of blank deformation and its projection, incorporating changes in gear blank stiffness, the gear blank deformation calculation model was established, and the model was verified by simulation and machining experiments, which lays a theoretical foundation for the prediction and control of the machining deformation of the segmented equal-base circle bevel gear.

2. Analysis of Gear Blank Deformation and Additional Torque

The profile of the tooth blank of a large equal-base bevel gear closely resembles a rectangle. With a substantial root angle and a large outer circle diameter, the tooth blank, post-splitting, can be effectively regarded as a cuboid. This study defines the length direction of the semi-finished product as the X direction (rolling direction), the lateral direction as the Y direction, and the thickness direction as the Z-axis, oriented vertically upward. For this processing and measurement test, 7075-t7451 aluminum alloy is employed. To ensure the finite element model accurately represents the residual stress distribution of the wheel blank, an appropriate function is designed to express the relationship between the thickness of the wheel blank and the calculated initial residual stress distribution characteristics [17]. Subsequently, the subroutine is designed, and the corresponding subroutine is invoked by ABAQUS software, establishing the finite element analysis model for the automatic continuous loading of residual stress.

The internal stress within the corresponding part dissipates when the material in the tooth space is removed, representing the fundamental aspect of the processing deformation of the split gear blank. Applying additional stress to the left and right sides of the tooth slot allows for an equivalent simulation of the influence of cutting on deformation. This approach facilitates the determination of torque and wheel blank deformation resulting from material removal. Figure 1 illustrates a cloud diagram depicting deformation during simulated processing. It can be observed from the cloud diagram that the processing area is small, and the deformation is the largest in other places. Furthermore, as one moves farther away from the cutting position, the deformation diminishes. Upon completion of the machining process, the gear blank adopts an overall curved state, with deformation symmetrically distributed in the X direction of the wheel blank.



(**a**) (**b**)

Figure 1. Deformation nephogram of simulated machining. Notes: (**a**) deformation nephogram of machining middle cogging; (**b**) deformation nephogram of finished machining.

If the curvature of the tooth line is not considered, the shape of the tooth blank after machining a tooth pitch is almost U-shaped in the X direction. The research shows that the maximum change in internal stress occurs in the length direction of the processed gear blank. At this time, the specific distribution of additional stress and the established coordinate system are shown in Figure 2. After removing the material, the initial support stress σ on the left and right sides of the tooth slot also disappears. In this case, applying stress $-\sigma$ to the sidewall of the tooth slot achieves the force-equivalent effect.

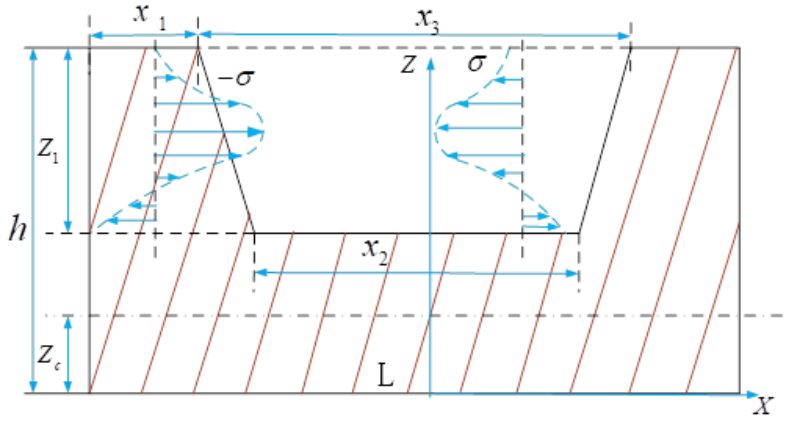


Figure 2. Diagram of additional bending stress.

In Figure 2, z_c is the position of the neutral axis, on which the centroid of the section is located. During the gear cutting process, the position of the centroid of the section changes continuously. Different additional stresses are created when the material is removed layer by layer from the tooth slot. The accumulation of additive stress and the initial residual stress of the part lead to the occurrence of the gear blank bending deformation. With the help of the relevant theory of material mechanics, the curvature can be calculated and combined with the additive stress distribution of bending in the process of gear processing.

The curvature change law, additional stress calculation formula, and residual stress balance expression of the gear before and after processing are solved in sequence. Finally, the formula for the additive torque due to the redistributed internal stress σ_{i1} located on the instantaneous neutral axis is calculated.

$$M = \int_0^{z_1} \sigma_{i1}(z)(z - z_c)\chi_2 dz \tag{1}$$

3. Calculation of Bending Deformation

To determine the precise numerical value of the bending deformation for the wheel blank with only one tooth groove and no helix angle, as depicted in Figure 2, an analysis of the additional torque is conducted. This analysis, combined with the machining characteristics of a single pitch, allows for the initial determination of the internal stress in each layer. Subsequently, the size parameters of the gear blank are substituted into Equation (1) to calculate the additional torque experienced by the gear blank during processing,

$$M = \int_0^{z_1} \sigma_{il}(z)(h - z_c - z) * [x_3 - (x_3 - x_2)(z_1/2.25m)]dz \tag{2}$$

where $x_1 = (L - x_3)/2$, m is the gear modulus.

Then, the additional moment is substituted into the calculation formula to obtain the X direction bending deformation of the wheel blank without the helix angle after machining a tooth slot:

$$S_i = \int_0^L x * M/(K_i L_i)dx \tag{3}$$

where K_i is the rigidity of the gear blank when the ith single tooth slot on the gear blank is processed. L_i is the length of the cantilever beam of each slot for qualitative analysis.

For equal-base circle bevel gear, due to the existence of the helix angle, the analysis model in Figure 2 must be established according to the normal sectional dimension of the midpoint of tooth length; that is, the bending deformation of the single tooth space obtained by Equation (3) is related to the helix angle and the direction of rotation. In order to determine the simplified calculation of the blank deformation of the split gear, the Y direction is consistent with the tangent direction of the tooth line at the midpoint of the tooth length, and the one perpendicular to it is set as the X direction. For the split gear blank of right-hand equal-base circle bevel gear, in the two-dimensional view from the top of the tooth (Figure 3), taking the rightmost tooth space as the analysis datum, it is more convenient to establish the plane reference coordinate system for the overall deformation analysis, and the analysis principle is the same for the left-hand gear. For the reference coordinate system, the deformation analysis plane coordinate system $O_iX_iY_i$ for machining each single tooth space, there are different inclination angles.

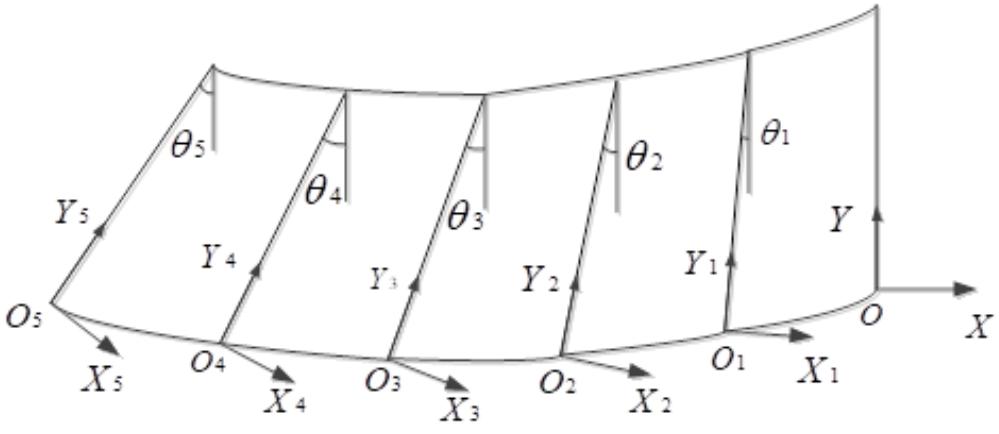


Figure 3. Two-dimensional diagram of gear blank.

For each tooth space in Figure 3, from the calculation method of equivalent stiffness derived, the stiffness of the gear blank when machining different tooth slots can be obtained, and it is set to K_{11}, K_{12}, K_{13}, K_{14}, and K_{15} in sequence according to the machining order. Based on the split structure of equal-base circle bevel gear and the machining process, the equivalent stiffness of the cutting gear blank is

$$K_i = \int_0^L EI_k(y_1(x)'')^2 dx \tag{4}$$

where $y_1(x)$ is the deflection curve equation of the equivalent equal section beam of the split gear blank. The stiffness is substituted into Equation (3) and the integration interval is adjusted; the deformation S_i in Z_i direction can be obtained via machining single tooth space at different positions. The deformation is located in the plane $X_iO_iZ_i$, and the angle between the plane $X_iO_iZ_i$ and the XOZ plane of the datum coordinate system is θ_i. Figure 4 shows the deformation projection diagram of the wheel blank.

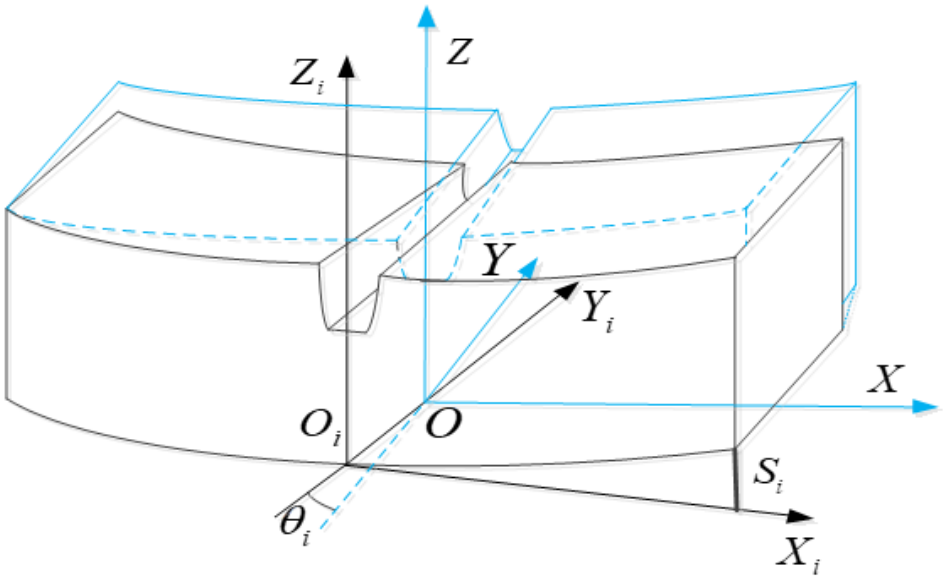


Figure 4. Projection diagram of gear blank deformation.

To solve the total deformation, the independent deformation of each tooth space is projected to the XOZ plane of the datum coordinate system, and then the deformation superposition calculation is performed. The principle of deformation projection is shown in Figure 5. After projection, the bending deformation S corresponding to S_i is obtained.

As shown in Figure 5, from bending deformation S_i to S the amount of bending deformation remains unchanged, but the length of the analysis unit changes. When it is projected to the plane OXZ of the datum coordinate system, there is an additional projection relationship of $cos(\theta_i)$.

$$L_i = L * \cos(\theta_i) \tag{5}$$

According to the former finite element analysis of wheel blank deformation, the deformation has nothing to do with the cutting sequence, and the bending deformation follows the law of deformation superposition. Without losing generality, the first machined tooth space starts from the third tooth space as shown in Figure 6.

The coordinate system $S_3(o_3 - x_3, z_3)$, as shown in the Figure 6, is established at the tooth space of the segmented gear blank, and z_3 is the axis of symmetry in the middle of the tooth slot. When machining the first tooth space, on the XOZ plane of the coordinate system OXYZ, θ_{11} and θ_{12} are the angles between the bottom surface of the left and right sides without the processing areas and the line which is horizontal, respectively.

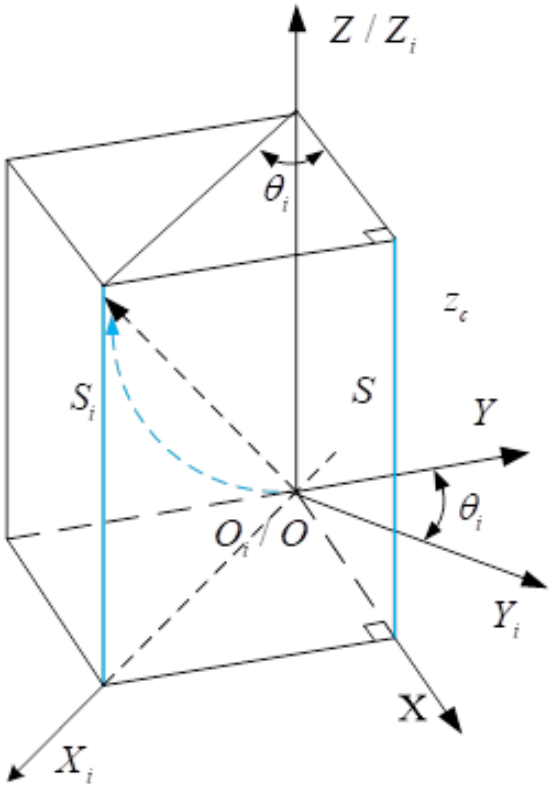


Figure 5. Projection principle diagram of gear blank deformation.

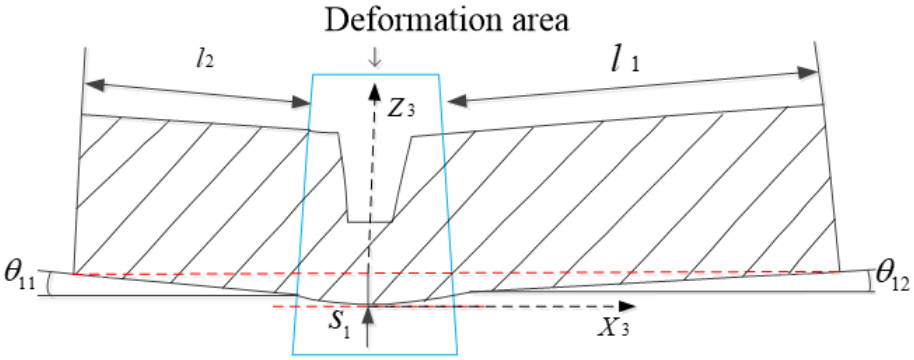


Figure 6. Effect drawing of machining deformation of the first tooth slot.

Because of the invariance of the bending deformation projection, S_1 can be obtained directly according to Equation (6).

$$S_1 = \int_0^{L_1} x * M/(K_1 L_1) dx \tag{6}$$

$$\theta_{11} \approx arc\sin(S_1/l_2) \tag{7}$$

$$\theta_{12} \approx arc\sin(S_1/l_1) \tag{8}$$

According to the above formulas and parameters, the additional torque of cutting one tooth space is calculated, which is substituted into the deflection calculation formula, and the calculation program is written in MATLAB (MATLAB R2014b (8.4.0.150421)) to obtain the gear blank deformation S_1, θ_{11}, and θ_{12}. At the same time, the finite element simulation is performed to simulate the machining process, and the specific ABAQUS simulation is shown in Figure 1a.

The results of finite element simulation and calculation method are summarized, and the precise data are shown in Table 1.

Table 1. Physical properties of air at atmospheric pressure.

Deformation	Data
S_1 from calculation	0.0230 mm
S_1 from simulation	0.0250 mm
θ_{11} from calculation	0.0176°
θ_{12} from calculation	0.0177°

Here, continue to process the tooth slot toward the left side of the wheel blank according to the set order, and set the local deformation of the wheel blank when the tooth slot is processed alone to be S_2, then the deflection angle of the left and right ends of the bottom surface caused by deformation are θ_{21} and θ_{22}, respectively.

$S_4(o_4 - x_4, z_4)$ is obtained through coordinate transformation at the position of the symmetry axis of the second tooth space. First, linearly move the coordinate system $S_3(o_3 - x_3, z_3)$, and then turn the coordinate system clockwise at a certain angle. The establishment and transformation process of the coordinate system is shown in Figure 7.

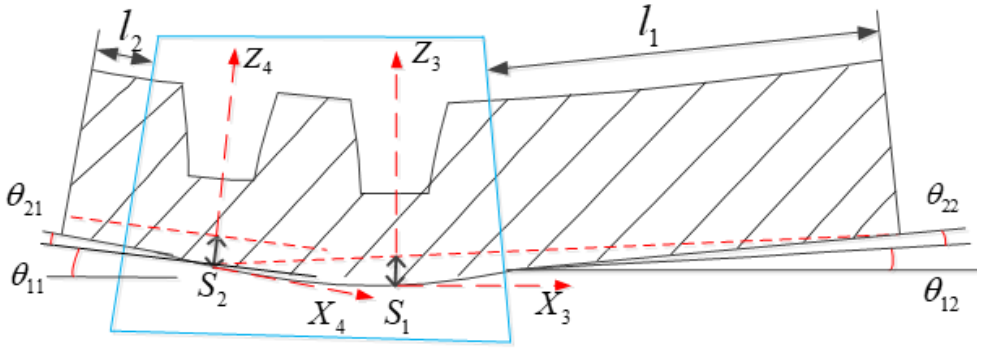


Figure 7. Schematic diagram of deformation after cutting the second slot.

The deformation direction corresponding to the second tooth space is perpendicular to the tangent direction of the deformed bottom surface of the first tooth space, and the deformation of the second tooth slot after single machining is S_2.

$$S_2 = \int_0^L x * M/(K_2 L_2) dx \tag{9}$$

The distance between the two tooth spaces is p in the non-machining state, and the total deformation after bending deformation composition is S.

$$S = S_2 * cos(\theta_{11}) + p * tan(\theta_{11}) \tag{10}$$

After machining the first two tooth slots, the angle between the corresponding bottom plane of the unprocessed area at the left end and the horizontal line is approximately $\theta_{11} + \theta_{21}$, and the bottom surface deflection angle of the unprocessed area at the right end is approximately $\theta_{12} + \theta_{22}$. Similarly, the deformation characteristics of the gear blank when two tooth slots are processed can be obtained. At the same time, the deformation is analyzed by finite element simulation, and the simulation results are shown in Figure 8.

The results of deformation calculation and simulation are summarized as shown in Table 2.

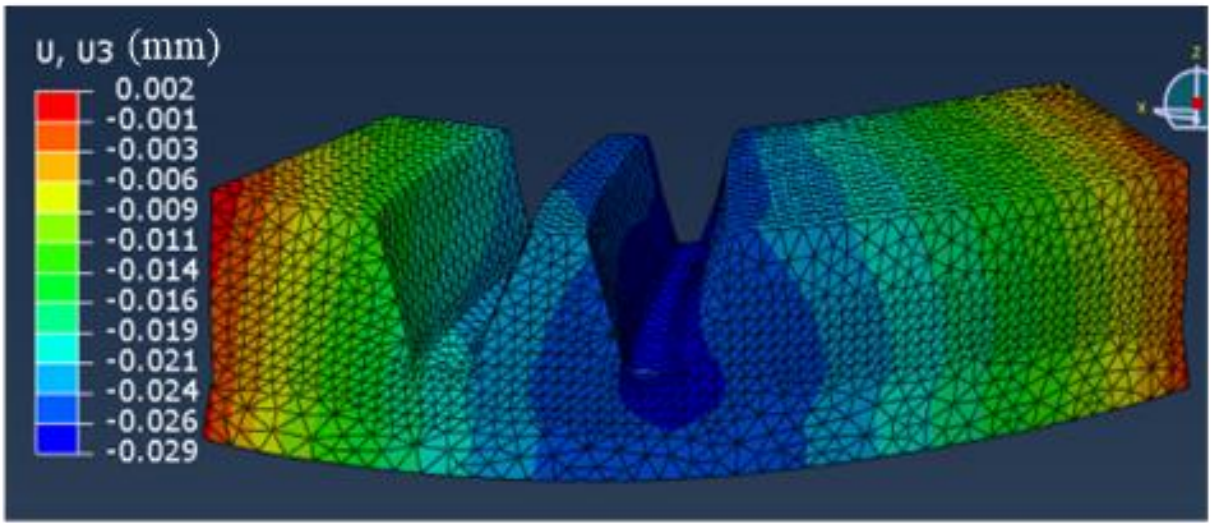


Figure 8. Simulation of cutting two slots.

Table 2. Deformation data after machining two tooth spaces.

Deformation	Data
S_1 from calculation	0.0275 mm
S_1 from simulation	0.0290 mm
$\theta_{11} + \theta_{21}$ from calculation	0.0286°
$\theta_{12} + \theta_{22}$ from calculation	0.0143°

Similarly, the deformation direction of the third tooth space, that is, the leftmost tooth space, is perpendicular to the tangent direction of the deformed bottom surface corresponding to the second tooth space, and the total deformation after machining the three left tooth spaces is

$$S = S_3 * cos(\theta_{11} + \theta_{21}) + p * (tan(\theta_{11}) + tan(\theta_{11} + \theta_{21})) \quad (11)$$

Further machining the right three tooth spaces, and so on, with the machining process, the bottom angle and deformation of the left and right sides after machining are as follows:

$$\theta_1 = \theta_{11} + \theta_{21} + \theta_{31} \quad (12)$$

and

$$S = S_4 * cos(\theta_1) + p * (tan(\theta_{11}) + tan(\theta_{11} + \theta_{21}) + tan(\theta_{11} + \theta_{21} + \theta_{31})) \quad (13)$$

After all the machining is completed, the deformation of split blank is shown in Figure 9. At the same time, the angle between the tangent line of the bottom surface of the left end and the horizontal line is set as θ_1, the angle between the straight line part of the right bottom surface and the horizontal line is set as θ_2, and the total superposition deformation is S.

At this point, the simulation of all the machining is completed, and the results are shown in Figure 1b. Table 3 shows the deformation data obtained by calculation and simulation.

Table 3. Deformation data after all machining.

Deformation	Data
S from calculation	0.039 mm
S from simulation	0.038 mm
θ_1 from calculation	0.030°
θ_2 from calculation	0.031°

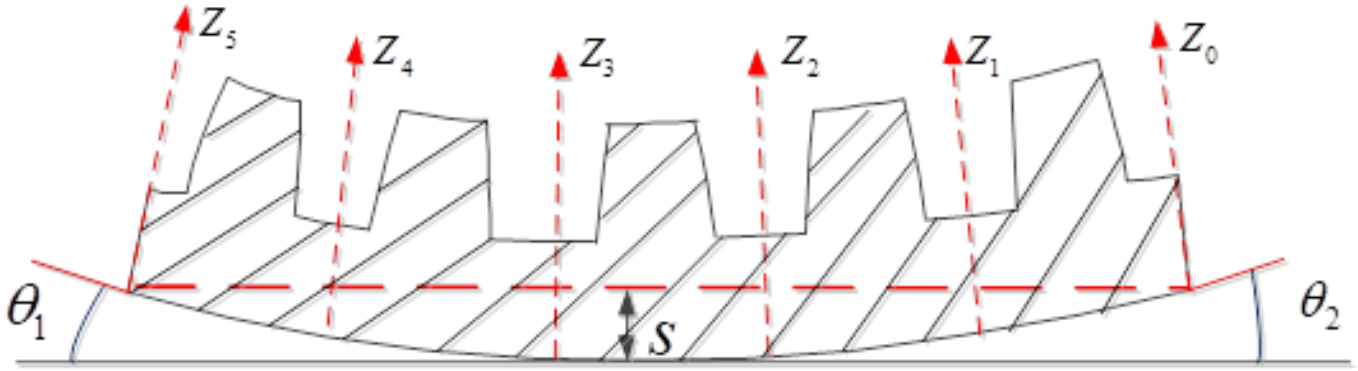


Figure 9. Deformation diagram after all machining.

According to the data in Table 3, the split equal-base circle bevel gear presents bending deformation after machining; the maximum deformation is at the central position of the gear blank, and the inclination angles of the left and right sides caused by the deformation are basically the same.

4. Experimental Section

In the experimental part, the flatness of the bottom surface, the verticality of the left and right end faces, and the diameter of the inner and outer circles of the wheel blank are measured, and the correctness of the previous theoretical calculation and finite element analysis are indirectly verified through the analysis of the change trend in these parameters.

Experimental verification is conducted using gears of the same material and specification as in the simulation. The main parameters of the split wheel blank are as follows: the inner and outer diameters are 626 mm and 804 mm, respectively, and the angle between the two end faces of the wheel blank is 36°. In conjunction with the aforementioned simulation process, experimental verification is conducted using a three-coordinate measuring machine. The specific steps are as follows: First, the initial measurement of the processed split blank is conducted on the CMM. Second, the first tooth slot is machined for the second measurement. Third, all the tooth slots on the right side of the blank are machined, and the third measurement is performed. Finally, all the tooth slots on the left are machined, and the fourth measurement is taken. Each measurement includes the following elements of the gear blank: the flatness of the bottom surface, the verticality of the left and right end faces, the diameter of the inner and outer circles, and the angle between the left and right end faces.

Figure 10 is the first measurement of the machined split gear blank. Figure 11a is the machining of the first tooth slot on the CNC machine, and Figure 11b is the second measurement of the machining of the first tooth slot.

Figure 11c shows the process of machining the right tooth slots on the CNC machine, and Figure 11d shows the third measurement after machining all the tooth slots on the right. Figure 11e shows all the tooth slots processed on the left side, and Figure 11f shows the process of fourth measurement.

According to the experimental design and measurement items, the gear blank is measured on the Hexagon CMM, measurements were taken multiple times at each stage of the experiment, and the data in Table 4 are processed arithmetic means. The specific measured values are shown in Table 4.

From the measurement results, the measurement data of the gear blank during the first measurement is small because the tooth slot has not been machined at this time. But with the progress of multiple processing and the position tolerances, the shape, inner and outer diameters of the gear blanks all change significantly. The flatness tolerance of gear blank has a large variation range, which indicates that the wheel blank has a large bending deformation. During the machining process, the included angle between the two end faces keeps decreasing, and the included angle after machining is 0.005° smaller than

that before machining, which shows that the gear blank will have opening deformation during machining. Moreover, the variation trend of perpendicularity tolerance of left and right end faces is opposite with the processing, which indicates that a certain amount of torsional deformation occurs along the *X*-axis of the gear blank and the deformation is mainly bending deformation after projection. The size of the outer circle is reduced by about 3 mm, which indicates that there is a large deformation in the Y direction. The data are consistent with the simulation results. The data in the third column of the table have a sudden change and do not coincide with the overall change trend, which can be the result of the measurement error.

Table 4. Experimental data.

Measurement	The 1st Measurement	The 2nd Measurement	The 3rd Measurement	The 4th Measurement
Bottom surface flatness (mm)	0.035	0.015	0.089	0.053
Perpendicularity of left end surface	0.003	0.017	0.024	0.026
Perpendicularity of right end face	0.029	0.026	0.005	0.017
Outer diameter (mm)	802.520	802.898	801.850	800.701
Inner diameter (mm)	625.292	625.222	625.675	625.006



Figure 10. First measurement.

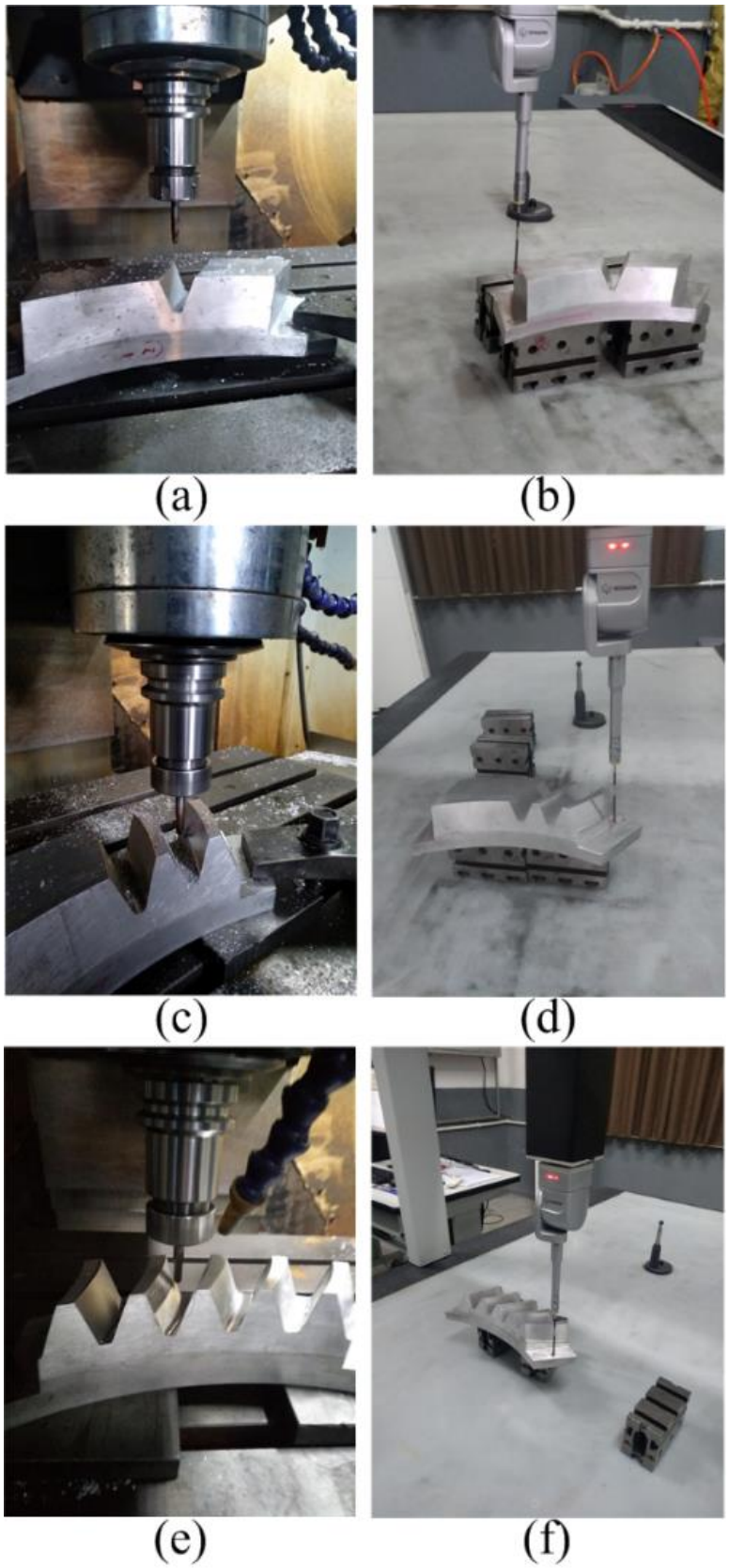


Figure 11. The process of machining all tooth space and the second to fourth measurement. Notes: (**a**) machining the 1st tooth space; (**b**) the 2nd measurement; (**c**) machining the right residual tooth space; (**d**) the 3rd measurement; (**e**) machining the left residual tooth space; (**f**) the 4th measurement.

5. Conclusions

The main research results and conclusions are summarized as follows:

1. Based on the analysis of the deformation and the additional stress during the machining of the segmented equal-base circle bevel gear, the calculation model of the additional torque in the residual material is established. On this basis, the bending deformation of the segmented equal-base circle bevel gear in machining single tooth slot is solved. The results show that for split curved bevel gears, the deformation of the wheel blank can be analyzed and calculated by deformation projection and superposition.
2. Through simulation and experimental research, the machining deformation calculation model proposed in this paper has been verified. The research also shows that for the workpiece, which is similar to the segmented gear blank, the deformation can be effectively predicted by establishing an accurate simulation model loaded with internal stress.

Author Contributions: Conceptualization, K.X. and B.W.; methodology, K.X. and Y.X.; software, W.X.; validation, K.X., B.W. and B.C.; formal analysis, W.X.; investigation, W.X. and Y.X.; resources, K.X.; data curation, K.X.; writing—original draft preparation, W.X.; writing—review and editing, K.X.; visualization, B.C.; supervision, K.X.; project administration, B.W.; funding acquisition, K.X. All authors have read and agreed to the published version of the manuscript.

Funding: This research was funded by The Key Scientific Research Projects of Colleges And Universities in Henan Province, grant number NO. 19A460020.

Institutional Review Board Statement: Not applicable.

Informed Consent Statement: Not applicable.

Data Availability Statement: The data presented in this study are available on request from the corresponding author. The data are not publicly available due to future research plans that require their use for ensuring the originality and integrity of forthcoming studies.

Conflicts of Interest: Authors Wen Xin and Bo Cheng was employed by the company CITIC Heavy Industries Co., Ltd. The remaining authors declare that the research was conducted in the absence of any commercial or financial relationships that could be construed as a potential conflict of interest.

Abbreviations

Symbol	Explanation
M	Additional torque during processing
σ_{i1}	Internal stress distribution
z	Vertical direction coordinate
z_c	Position of the neutral axis
h	Gear blank height
m	Gear module
x_1, x_2, x_3	Related to gear blank dimensions
L	Total length of gear blank
L_i	Length of cantilever beam for each slot
K_i	Stiffness of gear blank during processing
S_i	Deformation of gear blank
θ_i	Angle between bottom surface and horizontal line
$\theta_{11}, \theta_{12}, \theta_{21}, \theta_{22}$	Specific angles during different stages of processing
p	Tooth pitch
E	Elastic modulus
I_k	Moment of inertia of the cross-section

References

1. Zhang, W.H.; Gong, Y.P.; Wang, D. Tooth surface geometry and modification analysis of equal base bevel gear. *J. Northeast. Univ.* **2000**, *21*, 390–393.
2. Wang, B.; He, Y.P.; Feng, P.Y.; Sun, X.; Xu, A.J.; Li, J.B.; Li, T.X.; Jia, X.J.; Zhang, B. Digitized modeling and machining simulation of equal base bevel gear. *ITM Web Conf.* **2018**, *17*, 01015. [CrossRef]
3. Deng, J.; Wang, B.; Deng, X.Z.; Li, J.B. The theoretical and experimental research of machining equal base circle bevel gears with a pot-shaped milling cutter. *J. Adv. Mech. Des. Syst. Manuf.* **2015**, *9*, JAMDSM0041. [CrossRef]
4. Zhang, J.Q.; Zhang, Z.Y.; Zhang, Y.G. Design and application of manufacturing process of large-scale spiral bevel gear. *Manuf. Technol. Mach. Tool* **2014**, *5*, 84–86.
5. Wang, B.; Yan, C.X.; Feng, P.Y.; Wang, S.P.; Chen, S.; Cao, X.M. Prediction of machining deformation and reasonable design of gear blank for split straight bevel gear. *Int. J. Adv. Manuf. Technol.* **2022**, *119*, 2863–2875. [CrossRef]
6. Kang, Z.Z.; Teng, L.X. Manufacturing technology of split large gear. *Machinery* **1998**, *1*, 27–28.
7. Wang, B.; Yan, C.X.; Li, J.B.; Feng, P.Y.; Wang, S.P.; Chen, S.; Su, J.X. Residual Stress and Deformation Analysis in Machining Split Straight Bevel Gears. *Stroj. Vestn.—J. Mech. Eng.* **2021**, *67*, 114–122. [CrossRef]
8. Sun, J.; Ke, Y.L. Study on machining distortion of unitization airframe due to residual stress. *J. Mech. Eng.* **2005**, *41*, 117–122. [CrossRef]
9. Meng, L.H.; He, N.; Li, L. Caculation of residual stress induced by machining in internal surface of TC4 tubular parts and its FEA. *China Mech. Eng.* **2014**, *25*, 2583–2587.
10. Wang, Z.Q.; Li, J.F.; Sun, J.; Li, G.Y. FEA analysis of deformation correction by side-wall rolling of aircraft monolithtic components. *China Mech. Eng.* **2009**, *20*, 612–616.
11. Huang, X.M. Deformation Mechanism and Prediction of Aluminum Alloy Monolithic Component in the Milling. Ph.D. Thesis, Shandong University, Jinan, China, 2015.
12. Nervi, S.A. Mathematical Model for the Estimation of Effects of Residual Stresses in Aluminum Parts. Ph.D. Thesis, Washington University, St. Louis, MO, USA, 2005.
13. Keith, A.Y. Machining Induced Residual Stress and Distortion of Thin Parts. Ph.D. Thesis, Washington University, St. Louis, MO, USA, 2005.
14. Ratchev, S.; Liu, S.; Huang, W.; Becker, A.A. An advanced FEA based force induced error compensation strategy in milling. *Int. J. Mach. Tools Manuf.* **2005**, *46*, 542–551. [CrossRef]
15. Takayuki, A.; Tomohiro, S.; Hiroki, I. Plastic deformation mechanism of hypoid gears. *J. Adv. Mech. Des. Syst. Manuf.* **2017**, *1*, JAMDSM0069.
16. Mohd, S.A.A.; Tatsuaki, F.; Kazuhiro, K.; Shigeki, T.; Satoshi, A.; Akira, H.; Takashi, U. Residual stress and deformation of consolidated structure obtained by layered manufacturing process. *J. Adv. Mech. Des. Syst. Manuf.* **2013**, *7*, 244–256.
17. Wang, B.; Fan, M.; Yan, C.; Cao, X.; Li, T. Analysis of Stress and Deformation in Machining of Split Spiral Bevel Gear. *Mech. Sci. Technol.* **2022**, *41*, 1070–1075.

Disclaimer/Publisher's Note: The statements, opinions and data contained in all publications are solely those of the individual author(s) and contributor(s) and not of MDPI and/or the editor(s). MDPI and/or the editor(s) disclaim responsibility for any injury to people or property resulting from any ideas, methods, instructions or products referred to in the content.